

PathoHR: Breast Cancer Survival Prediction on High-Resolution Pathological Images

Yang Luo^{1*}, Shiru Wang^{2*}, Jun Liu^{3*}, Jiaxuan Xiao^{4*}, Rundong Xue⁵, Zeyu Zhang^{6†}, Hao Zhang⁷, Yu Lu⁸, Yang Zhao^{9‡}, Yutong Xie¹⁰

¹XJLTU, ²Dartmouth, ³NUP, ⁴DLMU, ⁵XJTU, ⁶ANU, ⁷UCAS, ⁸SZTU, ⁹La Trobe,
¹⁰MBZUAI

Abstract. Breast cancer survival prediction in computational pathology presents a remarkable challenge due to tumor heterogeneity. For instance, different regions of the same tumor in the pathology image can show distinct morphological and molecular characteristics. This makes it difficult to extract representative features from whole slide images (WSIs) that truly reflect the tumor’s aggressive potential and likely survival outcomes. In this paper, we present **PathoHR**, a novel pipeline for accurate breast cancer survival prediction that enhances any size of pathological images to enable more effective feature learning. Our approach entails (1) the incorporation of a *plug-and-play* high-resolution Vision Transformer (ViT) to enhance patch-wise WSI representation, enabling more detailed and comprehensive feature extraction, (2) the systematic evaluation of multiple advanced similarity metrics for comparing WSI-extracted features, optimizing the representation learning process to better capture tumor characteristics, (3) the demonstration that smaller image patches enhanced follow the proposed pipeline can achieve equivalent or superior prediction accuracy compared to raw larger patches, while significantly reducing computational overhead. Experimental findings validate that PathoHR provides the potential way of integrating enhanced image resolution with optimized feature learning to advance computational pathology, offering a promising direction for more accurate and efficient breast cancer survival prediction. Code will be available at <https://github.com/AIGeeksGroup/PathoHR>.

Keywords: High-resolution representations · Pathological imaging · Survival prediction.

1 Introduction

In breast cancer pathology, accurate survival prediction fundamentally relies on the detailed analysis of Whole Slide Images (WSIs), which capture representation morphological characteristics that indicate tumor aggressiveness and potential treatment outcomes [9,47]. The high-resolution nature of these pathological images provides essential visual information about cellular patterns, tissue organization, and tumor heterogeneity that directly correlate with patient

* Equal contribution. †Project lead. ‡Corresponding author: y.zhao2@latrobe.edu.au.

prognosis [23,24]. Recently, computational pathology has gained significant attention, with extensive research focusing on extracting and analyzing quantitative features from WSIs for survival prediction [29,8]. Despite notable advancements [21,19], cancer survival prediction remains challenging. The primary one lies in the significant tumor heterogeneity in pathology, where different regions of the same tumor exhibit distinct morphological characteristics, making it difficult to capture representative predictive patterns [22,26]. Besides, while high-resolution images contain detailed morphological information crucial for accurate prediction, processing such high-dimensional data demands substantial computational resources. Current approaches typically address this by cropping WSIs into smaller patches, but this creates another challenge: how to effectively learn and leverage the similarity features across different patches to capture the tumor's overall characteristics [10,44]. This fundamental tension between maintaining high-resolution information and learning representative features across patches has limited the achievement of optimal predictive performance in clinical settings [20,37].

To address these challenges, we propose **PathoHR**, a novel pipeline for breast cancer survival prediction that improves pathological image analysis through efficient multi-resolution processing and advanced feature representation learning. The contribution of this paper is threefold:

(1) A *plug-and-play* high-resolution Vision Transformer (ViT) framework is introduced for flexible patch-wise WSI enhancement, designed to process patch-based pathology image regardless of input size. The framework integrates seamlessly with existing architectures to enhance patch-based WSIs, enabling the extraction of fine-grained morphological details that are critical for survival prediction while maintaining computational efficiency.

(2) A systematic evaluation of advanced similarity metrics is adapted for contrastive learning, designed to effectively discriminate between common and distinct features across multiple tumor regions. This comprehensive evaluation framework aims to address the challenge of tumor heterogeneity by effectively capturing and leveraging common characters across different patches.

(3) A streamlined approach for processing enhanced smaller image patches is established, aimed at achieving superior prediction accuracy while reducing computational demands. The framework demonstrates how high-resolution feature learning using raw large patches can be effectively accomplished with smaller patches, providing a practical solution for clinical implementation.

2 Related Works

Representation Learning in Pathology. Representation learning has emerged as a crucial approach in computational pathology, particularly in enhancing the accuracy and efficiency of diagnostic models through advanced feature extraction techniques. Jaume et al. proposed the TANGLE framework, which leverages contrastive learning to align gene expression profiles with histology slide representations, significantly improving few-shot classification tasks [15].

Dynamic Resolution Adaptation in Vision Transformers. Dynamic resolution adaptation is a critical capability for Vision Transformers (ViTs) [36,40,16] in medical imaging [27,46], where image resolutions can vary significantly. Fan et al. introduced ViTAR, a Vision Transformer capable of processing images at any resolution through adaptive token merging and fuzzy position encoding [11]. This innovation significantly reduces computational costs while maintaining high accuracy, making it suitable for large-scale histology image analysis. Similarly, Sun et al. proposed HRNet (High-Resolution Network) [33], a framework that maintains high-resolution representations throughout the network, which is crucial for position-sensitive vision problems such as human pose estimation, semantic segmentation [38,30,12,31,41,35,43], and object detection [45,42,5,6]. Wang et al. proposed HRFormer, a high-resolution Transformer designed for dense prediction tasks, which maintains high-resolution representations throughout the network [34].

Feature Similarity in Whole Slide Images. The analysis of feature similarity in whole slide images (WSIs) is a critical aspect of digital pathology, enabling accurate classification and diagnosis [14,39]. Recent advancements in this domain have leveraged various techniques to enhance the representation and similarity assessment of features within WSIs. For instance, Bui et al. proposed FALFormer, a Transformer-based model that employs Nyström self-attention and feature-aware landmarks to capture the global relationships among patches in WSIs [4]. In addition, the HMIL framework, proposed by Jin et al., incorporates hierarchical multi-instance learning and supervised contrastive learning to address fine-grained classification tasks in WSIs [2].

3 Method

As presented in Fig.1, the proposed PathoHR pipeline comprises three integral components: (1) patch-wise feature extraction, (2) token merging via similarity computation for enhanced representation learning, and (3) *plug-and-play* ViT module to process multi-resolution patch-wise pathology images for better survival prediction.

3.1 Patch-wise Feature Extraction

The first step of the proposed pipeline involves processing whole slide images (WSIs) to extract low-dimensional representation features, details are shown in Fig. 1(1). Initially, each WSI is cropped into small patches of defined size. An Otsu’s method is applied to identify tissue boundaries and eliminate holes, ensuring only relevant tissue regions are retained for analysis. Following the prior work [25], a weakly supervised attention-based model with a pre-trained UNI encoder [7] is adopted for feature extraction. In total 1024-dim features for each patch are generated for further representation learning.

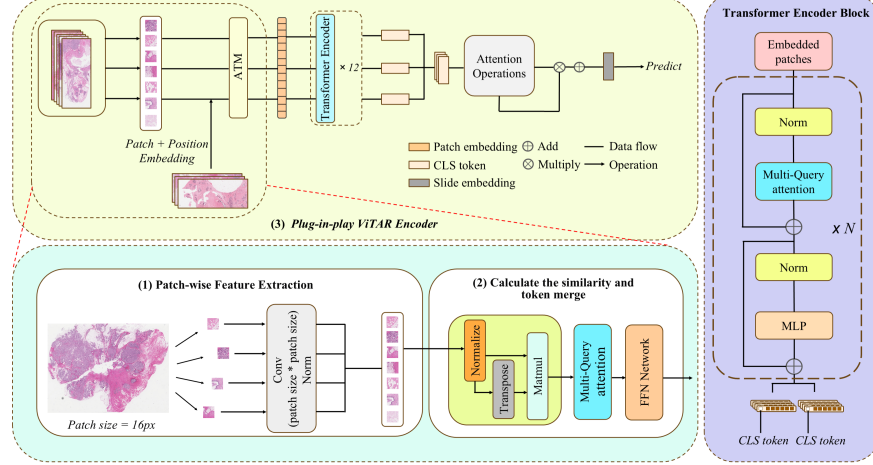


Fig. 1. The proposed PathoHR pipeline for breast cancer os prediction. The pipeline consists of three main components: (1) patch-wise feature extraction, (2) token merge similarity calculation for representation learning, and (3) a plug-and-play ViTAR encoder, that connects to the Transformer Encoder Block and incorporates Attention operations to generate predictive outputs.

3.2 Similarity Calculation for Token Merging

Following the concept of contrastive learning, where the model learns to identify and group similar features, several similarity computation methods are proposed and systematically tested. The details are presented in Fig. 1(2) and Fig. 2. **Pooled Attention Method.** Same as the ViTAR work [11], obtained through average pooling operations that reduce the sequence length by half. The similarity is computed through standard projection operations, where q , k , and v are derived from the input features x through a shared linear projection layer.

Euclidean Distance Method. This method [17] quantifies token relationships based on their spatial distances in the feature space. Details are shown in Fig. 2(1). After obtaining pooled queries, the similarity is computed as

$$sim(q, k) = \exp \left(- \sqrt{\sum_{i=1}^d (q_i - k_i)^2 \cdot \tau} \right) \quad (1)$$

where τ is a learnable temperature parameter that controls the sharpness of the similarity distribution. This distance-based approach captures local feature relationships in the embedding space.

Cosine Distance Method. In Fig. 2(2), a cosine distance method [18] is introduced. This method measures the angular correlation between token representations, focusing on directional relationships rather than absolute distances.

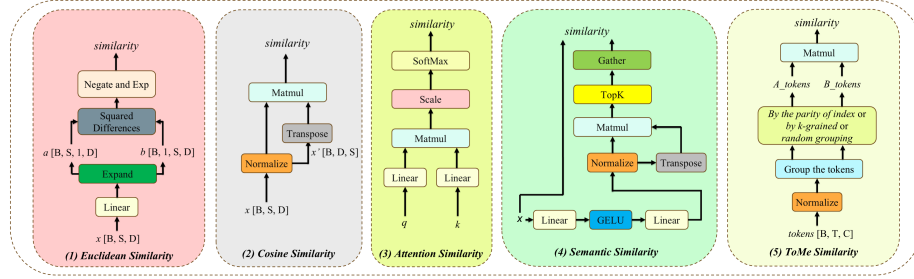


Fig. 2. This figure illustrates five different methods of calculating similarity: (1) Euclidean Similarity [17]; (2) Cosine Similarity [18]; (3) Attention Score [13]; (4) Semantic Similarity [32]; and (5) ToMe Similarity [3].

The similarity is calculated as

$$sim(q, k) = \tau \cdot \frac{q \cdot k}{\|q\| \cdot \|k\|} \quad (2)$$

where vectors are first normalized to unit length. The normalization ensures that the similarity measure is invariant to the scale of the token representations.

Attention Score Method. Attention score method [13] is introduced in Fig. 2(3) This method is built upon transformer architecture which benefits from the attention mechanism. The scaled dot-product attention with separate projections for queries, keys, and values are implemented in this work. The similarity is computed as

$$sim(q, k) = \text{softmax} \left(\tau \cdot \frac{q k^T}{\sqrt{d}} \right) \quad (3)$$

where d represents the feature dimension.

Semantic Similarity Method. The semantic similarity [32] introduces an additional layer of abstraction by projecting tokens through a lower-dimensional semantic space. The aim is to capture higher-level semantic relationships between tokens through learned transformations. This method is shown in Fig. 2(4). The similarity is calculated as

$$sim(q, k) = \text{softmax} \left(\frac{f_q(q) \cdot f_k(k)^T}{\sqrt{d}} \right) \quad (4)$$

where f_q and f_k are non-linear projection functions implemented as multi-layer perceptrons.

ToMe Similarity Method. This method [3] reduces the use of computational resource usage and maintains model performance by applying a token merging strategy based on bipartite soft matching. The architectural design is shown in Fig. 2(5) and aims to reduce computational overhead in similarity measurement by eliminating redundant token participation, thereby achieving optimized

computational density during large-scale token processing. The similarity is calculated as

$$sim(q, k) = \text{softmax} \left(G_A(t) \cdot G_B(t)^T \right) \quad (5)$$

where $G_A(t)$ and $G_B(t)$ are two tokens formed by grouping input tokens according to certain rules.

3.3 *Plug-in-play* ViTAR Encoder

The *plug-in-play* ViTAR Encoder contains mainly two parts as shown in Fig. 1(3): Adaptive Token Merge (ATM) and Fuzzy Positional Encodings (FPE) [11]. ATM starts by calculating the similarities among patches. Then these similarities are served as a query in a cross-attention operation to merge all features. This similarity-based token merging adaptively reduces spatial dimensions while preserving essential features. The FPE mechanism further reinforces resolution robustness by introducing controlled positional uncertainty. Specifically, for a token at position (i, j) , its fuzzy positional encoding P_f is computed as:

$$P_f(i, j) = P(i + s_1, j + s_2), \quad s_1, s_2 \sim \mathcal{U}(-0.5, 0.5) \quad (5)$$

where P represents the learnable positional embeddings, and U denotes uniform distribution. Through this dual-mechanism architecture, ViTAR could efficiently process multi-resolution inputs by adaptively managing token density while maintaining spatial coherence, ensuring consistent performance across varying image scales.

After ViTAR Encoder processes the input images and generates token representations, these tokens are further refined through the attention mechanisms of the Tangle architecture [15] to extract diagnostically relevant features. The pre-attention module applies multiple linear transformations with normalization and GELU activation to prepare patch features for attention computation. The gated-attention mechanism then employs a dual-path architecture where features are processed through parallel tanh and sigmoid activations before being multiplied together. This multiplication generates attention weights that highlight important features such as diagnostic regions in the slide. The slide embedding is generated by weighting patch features with these attention scores and then applying mean aggregation. This allows the model to emphasize diagnostically relevant regions while suppressing less informative areas.

The detailed implementation steps of the proposed PathoHR pipeline are formally defined in Algorithm 1, which outlines the end-to-end procedure. The inputs are WSI, patch size, similarity threshold for token merging (τ), transformer encoder block count (N), and transformer encoder iteration count (J). The output is overall survival (OS) prediction.

Algorithm 1 PathoHR: Multi-resolution Patch-based Pathology Image process

```

1: procedure PATHOHR(WSI,  $patch\_size$ ,  $\tau$ ,  $N$ ,  $J$ ,  $method$ )
2:    $tissue\_mask \leftarrow$  OtsuThreshold(WSI)
3:    $patches \leftarrow$  ExtractPatches(WSI,  $tissue\_mask$ ,  $patch\_size$ )
4:    $patch\_embeddings \leftarrow$  UNIEncoder( $patches$ )
5:    $CLS\_token \leftarrow$  InitializeCLSToken()
6:    $tokens \leftarrow$  Concatenate( $CLS\_token$ ,  $patch\_embeddings$ )
7:   for  $j = 1$  to  $J$  do
8:      $norm\_tokens \leftarrow$  Normalize( $tokens$ )
9:      $tokens \leftarrow tokens + MultiQueryAttention(norm\_tokens)$ 
10:     $tokens \leftarrow tokens + Linear(norm\_tokens)$ 
11:     $tokens \leftarrow TransformerEncoderBlocks(tokens, N)$ 
12:   end for
13:    $Q, K \leftarrow$  ProjectionHead( $tokens$ )
14:    $similarity\_matrix \leftarrow$  ComputeSimilarity( $Q, K, method$ )  $\triangleright$   $method \in \{Pooled$ 
Attention, Euclidean, Cosine, Attention Score, Semantic $\}$ 
15:    $merged\_tokens \leftarrow$  TokenMerge( $tokens, similarity\_matrix, \tau$ )
16:    $slide\_embedding \leftarrow$  ExtractCLSToken( $merged\_tokens$ )
17:    $output\_logits \leftarrow$  PredictionHead( $slide\_embedding$ )
18:    $prediction \leftarrow$  Classify( $output\_logits$ )
19:   return  $prediction$ 
20: end procedure

```

4 Experiments

4.1 Dataset and Evaluation Metrics

Dataset. We utilized a comprehensive dataset comprising 1,036 Whole Slide Images (WSIs) with corresponding OS labels from the **TCGA-BRCA** (Invasive breast cancer) dataset [1]. To facilitate comparative analysis, each WSI was segmented into 16×16 pixel patches. The dataset was randomly partitioned into training, validation, and testing sets with a ratio of 8:1:1, respectively.

Evaluation Metrics. Model performance was evaluated by comparing the prediction metrics which include AUC and ACC and F1 Recall and Precision between our proposed 16×16 patches and the baseline 24×24 patches, maintaining consistent model architecture across experiments. We employed a supervised learning strategy focused on minimizing mean square error loss. All experiments were performed on a standardized platform using a workstation equipped with an NVIDIA RTX A6000 GPU.

4.2 Comparative Study

We conducted a comparative analysis of our proposed PathoHR pipeline performance against benchmark Tangle methods without VITAR encoder enhancement. The validation results for intra-modality slide self-supervised learning (Intra) across different patch sizes and similarity metrics are presented in Table 1. Intra (24) and Intra (16) utilize the basic Tangle model, while the remaining results follow the proposed PathoHR pipeline with a patch size of 16×16 . The



Fig. 3. Performance on breast cancer classification task. Different models using WSIs as input for breast cancer classification tasks are evaluated. AUC values are reported.

results demonstrate that while smaller input patches intuitively lead to lower os prediction accuracy, our proposed PathoHR pipeline effectively counters this limitation. By enhancing representation feature extraction, the pipeline enables 16×16 patches to surpass the baseline architecture using 24×24 patches in both AUC and F1 scores.

Performance comparisons between our proposed PathoHR pipeline and architectures with different backbones performing similar classification tasks are also conducted [28]. Fig. 3. demonstrates that the PathoHR pipeline enables superior classification performance despite using relatively smaller patches, highlighting the efficiency of this approach.

4.3 Ablation Study

Table 1. Validation performance on os prediction for breast cancer pathology.(24) and (16) denote input patch sizes of 24×24 and 16×16 , respectively.

Models	AUC	ACC	F1	Recall	Precision
Intra(24)	0.8	0.95313	0.83025	0.95313	0.90845
Intra(16)	0.76786	0.97436	0.91077	0.87179	0.89451
Intra with pool	0.71622	0.94872	0.92375	0.94872	0.90007
Intra with cos	0.90741	0.97436	0.96170	0.97436	0.94938
Intra with euclidean	0.82413	0.97436	0.92375	0.94872	0.92915
Intra with semantic	0.90541	0.89286	0.92375	0.89286	0.94938
Intra with attention score	0.62353	0.94872	0.92375	0.94872	0.90007
Intra with ToMe	0.78947	0.97436	0.96170	0.97436	0.94938

Table 2 showcases the enhancements brought about by our proposed PathoHR strategies. The results indicate that integrating residual connections or similarity comparisons independently could improve os prediction accuracy. However, the experiments reveal a potential counteractive relationship between these components. Optimal results are achieved either using cosine similarity without residual connections or using only pooling with residual links. Future work should explore this interaction effect to potentially combine residual connections with selective similarity metrics for improved pathology-based survival prediction.

Table 2. Ablation study of different designs. Similarity matrix values are reported. Test performance on breast cancer os prediction is statistically evaluated.

Models	AUC	ACC	F1	Recall	Precision
Intra with 16	0.68235	0.74359	0.76476	0.74359	0.78757
Pool(only with res)	0.83118	0.76003	0.81796	0.76003	0.87533
Cosine	0.64815	0.87179	0.88615	0.87179	0.85207
Semantic	0.62037	0.89744	0.88615	0.89744	0.85207
Pool without res	0.73030	0.88462	0.83090	0.88462	0.78403
Cos without res	0.70142	0.89745	0.84616	0.89745	0.84221
Semantic without res	0.72294	0.88462	0.83090	0.88462	0.78403
ToMe	0.81429	0.87179	0.96154	0.84615	0.88552
ToMe without res	0.58571	0.92308	0.88615	0.92308	0.85207

5 Conclusion

In this paper, we present PathoHR, a novel pipeline for efficient multi-resolution processing of patch-based pathology images to improve representation learning. By leveraging diverse similarity metrics for adaptive token merging, our approach effectively clusters features based on their semantic relationships. Integrating the proposed plug-in-play ViTAR encoder alongside the Tangle model enables the use of smaller patches while achieving superior performance compared to prior large-patch approaches. The contributions of this study pave the way for fast and accurate os prediction using high-resolution pathology images. Future work might include the incorporation of multi-modal data to further enhance OS prediction accuracy.

References

- 13, B..W.H..H.M.S.C.L...P.P.J..K.R., data analysis: Baylor College of Medicine Creighton Chad J. 22 23 Donehower Lawrence A. 22 23 24 25, G., for Systems Biology Reynolds Sheila 31 Kreisberg Richard B. 31 Bernard Brady 31 Bressler Ryan 31 Erkkila Timo 32 Lin Jake 31 Thorsson Vesteinn 31 Zhang Wei 33 Shmulevich Ilya 31, I., et al.: Comprehensive molecular portraits of human breast tumours. *Nature* **490**(7418), 61–70 (2012)

2. et al., C.J.: Hmil: Hierarchical multi-instance learning for fine-grained whole slide image classification. *IEEE Transactions on Medical Imaging* (2024). <https://doi.org/10.1109/TMI.2024.3520602>
3. Bolya, D., et al.: Token merging for memory-efficient vision transformers. *arXiv preprint arXiv:2210.09461* (2022)
4. Bui, D.C., Vuong, T.T.L., Kwak, J.T.: Falformer: Feature-aware landmarks self-attention for whole-slide image classification. In: *Proceedings of Medical Image Computing and Computer Assisted Intervention – MICCAI 2024*. vol. LNCS 15004, pp. 123 – 132. Springer Nature Switzerland (October 2024)
5. Cai, G., Cai, Y., Zhang, Z., Cao, Y., Wu, L., Ergu, D., Liao, Z., Zhao, Y.: Medical ai for early detection of lung cancer: A survey. *arXiv preprint arXiv:2410.14769* (2024)
6. Cai, G., Zhang, R., He, H., Zhang, Z., Ergu, D., Cao, Y., Zhao, J., Hu, B., Liao, Z., Zhao, Y., et al.: Msdet: Receptive field enhanced multiscale detection for tiny pulmonary nodule. *arXiv preprint arXiv:2409.14028* (2024)
7. Chen, R.J., Ding, T., Lu, M.Y., Williamson, D.F., Jaume, G., Chen, B., Zhang, A., Shao, D., Song, A.H., Shaban, M., et al.: Towards a general-purpose foundation model for computational pathology. *Nature Medicine* (2024)
8. Cui, M., Zhang, D.Y.: Artificial intelligence and computational pathology. *Laboratory Investigation* **101**(4), 412–422 (2021)
9. El Nahhas, O.S., van Treeck, M., Wölflein, G., Unger, M., Ligero, M., Lenz, T., Wagner, S.J., Hewitt, K.J., Khader, F., Foersch, S., et al.: From whole-slide image to biomarker prediction: end-to-end weakly supervised deep learning in computational pathology. *Nature Protocols* **20**(1), 293–316 (2025)
10. Fan, L., Sowmya, A., Meijering, E., Song, Y.: Cancer survival prediction from whole slide images with self-supervised learning and slide consistency. *IEEE Transactions on Medical Imaging* **42**(5), 1401–1412 (2022)
11. Fan, Q., You, Q., Han, X., Liu, Y., Tao, Y., Huang, H., He, R., Yang, H.: Vitar: Vision transformer with any resolution. *arXiv preprint arXiv:2403.18361* (2024)
12. Ge, J., Zhang, Z., Phan, M.H., Zhang, B., Liu, A., Zhao, Y.: Esa: Annotation-efficient active learning for semantic segmentation. *arXiv preprint arXiv:2408.13491* (2024)
13. He, K., et al.: Transformers in medical image analysis. *Intelligent Medicine* **2**(3), 135–144 (2022)
14. Hiwase, A.D., Ovenden, C.D., Kaukas, L.M., Finnis, M., Zhang, Z., O'Connor, S., Foo, N., Reddi, B., Wells, A.J., Ellis, D.Y.: Can rotational thromboelastometry rapidly identify theragnostic targets in isolated traumatic brain injury? *Emergency Medicine Australasia* **37**(1), e14480 (2025)
15. Jaume, G., Oldenburg, L., Vaidya, A., Chen, R.J., Williamson, D.F., Peeters, T., Song, A.H., Mahmood, F.: Transcriptomics-guided slide representation learning in computational pathology. In: *Proceedings of the IEEE/CVF Conference on Computer Vision and Pattern Recognition (CVPR)*. pp. 9632–9644 (2024)
16. Ji, Y., Saratchandran, H., Gordon, C., Zhang, Z., Lucey, S.: Sine activated low-rank matrices for parameter efficient learning. *arXiv e-prints* pp. arXiv-2403 (2024)
17. Jones, A.R., et al.: Spatial analysis of histology in 3d: quantification and visualization of organ and tumor level tissue environment. *Heliyon* **8**(1), e08762 (2022)
18. Khan, M.H., et al.: A similarity measure of histopathology images by deep embeddings. *arXiv preprint arXiv:2107.13703* (2021)
19. Levy, J., Haudenschild, C., Barwick, C., Christensen, B., Vaickus, L.: Topological feature extraction and visualization of whole slide images using graph neural

networks. In: *BIOCOMPUTING 2021: Proceedings of the Pacific Symposium*. pp. 285–296. World Scientific (2020)

20. Li, B., Liu, F., Lv, B., Zhang, Y., Gou, F., Wu, J.: Cytopathology image analysis method based on high-resolution medical representation learning in medical decision-making system. *Complex & Intelligent Systems* **10**(3), 4253–4274 (2024)
21. Li, X., Li, C., Rahaman, M.M., Sun, H., Li, X., Wu, J., Yao, Y., Grzegorzek, M.: A comprehensive review of computer-aided whole-slide image analysis: from datasets to feature extraction, segmentation, classification and detection approaches. *Artificial Intelligence Review* **55**(6), 4809–4878 (2022)
22. Lim, B., Hortobagyi, G.N.: Current challenges of metastatic breast cancer. *Cancer and Metastasis Reviews* **35**, 495–514 (2016)
23. Liu, T., Su, R., Sun, C., Li, X., Wei, L.: Eocsa: Predicting prognosis of epithelial ovarian cancer with whole slide histopathological images. *Expert Systems with Applications* **206**, 117643 (2022)
24. Liu, X., Liu, Z., Yan, Y., Wang, K., Wang, A., Ye, X., Wang, L., Wei, W., Li, B., Sun, C., et al.: Development of prognostic biomarkers by tmb-guided wsi analysis: a two-step approach. *IEEE Journal of Biomedical and Health Informatics* **27**(4), 1780–1789 (2023)
25. Lu, M.Y., Williamson, D.F., Chen, T.Y., Chen, R.J., Barbieri, M., Mahmood, F.: Data-efficient and weakly supervised computational pathology on whole-slide images. *Nature Biomedical Engineering* **5**(6), 555–570 (2021)
26. Margolin, A.A., Bilal, E., Huang, E., Norman, T.C., Ottestad, L., Mecham, B.H., Sauerwine, B., Kellen, M.R., Mangravite, L.M., Furia, M.D., et al.: Systematic analysis of challenge-driven improvements in molecular prognostic models for breast cancer. *Science translational medicine* **5**(181), 181re1–181re1 (2013)
27. Qi, X., Zhang, Z., Handoko, A.B., Zheng, H., Chen, M., Huy, T.D., Phan, V.M.H., Zhang, L., Cheng, L., Jiang, S., et al.: Projectedex: Enhancing generation in explainable ai for prostate cancer. *arXiv preprint arXiv:2501.01392* (2025)
28. Qi, X., Zhang, Z., Zheng, H., Chen, M., Kutaiba, N., Lim, R., Chiang, C., Tham, Z.E., Ren, X., Zhang, W., et al.: Medconv: Convolutions beat transformers on long-tailed bone density prediction. *arXiv preprint arXiv:2502.00631* (2025)
29. Song, A.H., Jaume, G., Williamson, D.F., Lu, M.Y., Vaidya, A., Miller, T.R., Mahmood, F.: Artificial intelligence for digital and computational pathology. *Nature Reviews Bioengineering* **1**(12), 930–949 (2023)
30. Tan, S., Xue, R., Luo, S., Zhang, Z., Wang, X., Zhang, L., Ergu, D., Yi, Z., Zhao, Y., Cai, Y.: Segkan: High-resolution medical image segmentation with long-distance dependencies. *arXiv preprint arXiv:2412.19990* (2024)
31. Tan, S., Zhang, Z., Cai, Y., Ergu, D., Wu, L., Hu, B., Yu, P., Zhao, Y.: Segstitch: Multidimensional transformer for robust and efficient medical imaging segmentation. *arXiv preprint arXiv:2408.00496* (2024)
32. Tizhoosh, H., et al.: On image search in histopathology. *Medical Image Analysis* **87**, 102372 (2024)
33. Wang, J., Sun, K., Cheng, T., Jiang, B., Deng, C., Zhao, Y., Liu, D., Mu, Y., Tan, M., Wang, X., et al.: Deep high-resolution representation learning for visual recognition. *IEEE transactions on pattern analysis and machine intelligence* **43**(10), 3349–3364 (2020)
34. Wang, X., Yang, S., Zhang, J., Wang, M., Zhang, J., Yang, W., Huang, J., Han, X.: Transformer-based unsupervised contrastive learning for histopathological image classification. *Med. Image Anal.* **81**, 102559 (2022)

35. Wu, B., Xie, Y., Zhang, Z., Ge, J., Yaxley, K., Bahadir, S., Wu, Q., Liu, Y., To, M.S.: Bhsd: A 3d multi-class brain hemorrhage segmentation dataset. In: International Workshop on Machine Learning in Medical Imaging. pp. 147–156. Springer (2023)
36. Wu, B., Xie, Y., Zhang, Z., Phan, M.H., Chen, Q., Chen, L., Wu, Q.: Xlip: Cross-modal attention masked modelling for medical language-image pre-training. arXiv preprint arXiv:2407.19546 (2024)
37. Yu, X., Yang, Q., Zhou, Y., Cai, L.Y., Gao, R., Lee, H.H., Li, T., Bao, S., Xu, Z., Lasko, T.A., et al.: Unest: local spatial representation learning with hierarchical transformer for efficient medical segmentation. *Medical Image Analysis* **90**, 102939 (2023)
38. Zhang, R., Guo, H., Zhang, Z., Yan, P., Zhao, S.: Gamed-snake: Gradient-aware adaptive momentum evolution deep snake model for multi-organ segmentation. arXiv preprint arXiv:2501.12844 (2025)
39. Zhang, Z., Ahmed, K.A., Hasan, M.R., Gedeon, T., Hossain, M.Z.: A deep learning approach to diabetes diagnosis. In: Asian Conference on Intelligent Information and Database Systems. pp. 87–99. Springer (2024)
40. Zhang, Z., Qi, X., Chen, M., Li, G., Pham, R., Qassim, A., Berry, E., Liao, Z., Siggs, O., McLaughlin, R., et al.: Jointvit: Modeling oxygen saturation levels with joint supervision on long-tailed octa. In: Annual Conference on Medical Image Understanding and Analysis. pp. 158–172. Springer (2024)
41. Zhang, Z., Qi, X., Zhang, B., Wu, B., Le, H., Jeong, B., Liao, Z., Liu, Y., Verjans, J., To, M.S., et al.: Segreg: Segmenting oars by registering mr images and ct annotations. In: 2024 IEEE International Symposium on Biomedical Imaging (ISBI). pp. 1–5. IEEE (2024)
42. Zhang, Z., Yi, N., Tan, S., Cai, Y., Yang, Y., Xu, L., Li, Q., Yi, Z., Ergu, D., Zhao, Y.: Meddet: Generative adversarial distillation for efficient cervical disc herniation detection. In: 2024 IEEE International Conference on Bioinformatics and Biomedicine (BIBM). pp. 4024–4027. IEEE (2024)
43. Zhang, Z., Zhang, B., Hiwase, A., Barras, C., Chen, F., Wu, B., Wells, A.J., Ellis, D.Y., Reddi, B., Burgan, A.W., To, M.S., Reid, I., Hartley, R.: Thin-thick adapter: Segmenting thin scans using thick annotations. OpenReview (2023)
44. Zhao, L., Hou, R., Teng, H., Fu, X., Han, Y., Zhao, J.: Coads: Cross attention based dual-space graph network for survival prediction of lung cancer using whole slide images. *Computer Methods and Programs in Biomedicine* **236**, 107559 (2023)
45. Zhao, R., Zhang, Z., Xu, Y., Yao, Y., Huang, Y., Zhang, W., Song, Z., Chen, X., Zhao, Y.: Peddet: Adaptive spectral optimization for multimodal pedestrian detection. arXiv preprint arXiv:2502.14063 (2025)
46. Zhao, Y., Liao, Z., Liu, Y., Nijhuis, K.O., Barvelink, B., Prijs, J., Colaris, J., Wijffels, M., Reijman, M., Zhang, Z., et al.: A landmark-based approach for instability prediction in distal radius fractures. In: 2024 IEEE International Symposium on Biomedical Imaging (ISBI). pp. 1–5. IEEE (2024)
47. Zheng, Q., Yang, R., Ni, X., Yang, S., Xiong, L., Yan, D., Xia, L., Yuan, J., Wang, J., Jiao, P., et al.: Accurate diagnosis and survival prediction of bladder cancer using deep learning on histological slides. *Cancers* **14**(23), 5807 (2022)